

On applications of high-frequency asymptotics in aeroacoustics

BY N. PEAKE

*Department of Applied Mathematics and Theoretical Physics,
Centre for Mathematical Sciences, University of Cambridge,
Wilberforce Road, Cambridge CB3 0WA, UK*

Published online 28 January 2004

The aim of this paper is to survey a range of applications of high-frequency asymptotic methods in aeroacoustics. Specifically, we are concerned with problems associated with noise generation, propagation and scattering as found in large modern aeroengines. With regard to noise generation, we consider the interaction between high-frequency vortical waves and thin aerofoils, with particular emphasis being placed on the way in which the vortical waves act on the non-uniform mean flow around the aerofoil. A ray-theoretic description of the resulting sound as it propagates along the engine intake is then presented, followed by consideration of the diffraction of these rays by the (possibly asymmetric) intake lip to produce sound in the far field. A range of more detailed possible extensions is also presented.

Keywords: aeroacoustics; ray theory; sound generation; asymptotics

1. Introduction

The aim of this paper is to describe a range of applications of high-frequency asymptotics within the field of aeroacoustics, especially with regard to the prediction of noise generation by aeroengines. From an academic point of view, the extreme flow conditions, high speeds and complex geometries make this a fruitful area for the application of a rich variety of mathematical and computational techniques. In practical terms, the continued pressure for reduced community noise levels on the one hand and the high costs of redesign and in-service modification on the other drive the industrial imperative for accurate noise-prediction methods. There is no doubt that the fully computational solution of the governing equations will eventually provide the best route to a practical engineering tool, but a more analytical, and in particular asymptotic, approach can be helpful as well. A range of approaches that shed light on different aspects of the problem at hand will be considered here.

The first point to make is that the typical acoustic frequencies involved in this problem are high. For instance, the rotating blade rows generate tonal noise at frequencies equal to an integer multiple of $B\Omega_{\text{rot}}$, where Ω_{rot} is the shaft rotation rate and B is the number of blades (which is large, usually between 20 and 30), leading to frequencies of interest well into the kHz range and wavelengths many times smaller

One contribution of 13 to a Theme 'Short-wave scattering'.

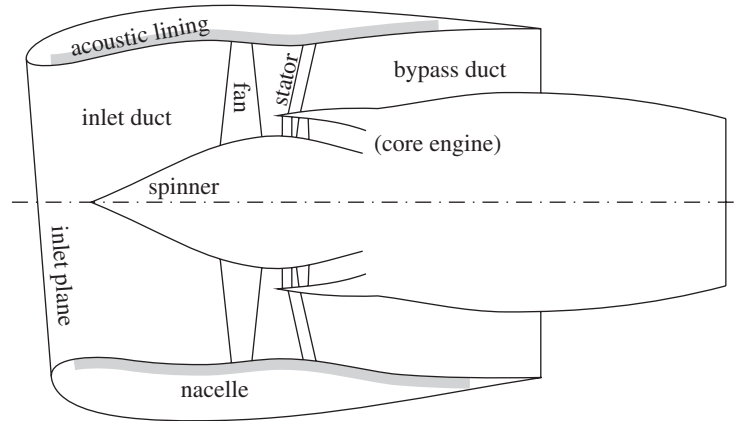


Figure 1. Schematic of a modern turbofan engine.
(Reproduced with permission from Dr S. W. Rienstra.)

than typical gross length-scales (such as the radius of the engine duct). Broadband noise is also generated, much of it at similarly high frequency. The second point is that the aeroacoustics can be broken down into two elements—the noise generation itself, and the propagation of that noise through the engine and out to the far field—and both aspects are amenable to asymptotic analysis.

A schematic of a modern turbofan engine is shown in figure 1. There are many different sources of noise, but one of the most significant and troublesome arises from the wakes shed by the rotating fan as they interact with the downstream stator blades. (This sort of rotor–stator interaction noise is also generated inside the core of the engine, by the compressor and turbine). The noise will escape to the far field, both downstream along the bypass duct and upstream through the fan and the inlet. In this paper we will review analytical high-frequency asymptotic calculations of the noise generation by the wake–stator interaction, and describe its propagation through the engine ducts and its scattering by the inlet lip en route to the far field.

The fundamental equation for sound generation by a body moving in flow was derived by Ffowcs Williams & Hawkings (1969), as an exact rearrangement of the Navier–Stokes equations. The Ffowcs Williams–Hawkings equation can be written in the form

$$\nabla^2 p' - \frac{1}{c_0^2} \frac{\partial^2 p'}{\partial t^2} = \mathcal{S}(\mathbf{x}, t), \quad (1.1)$$

where $p'(\mathbf{x}, t)$ is the unsteady (acoustic) pressure and c_0 is the uniform sound speed of the medium at infinity. The source term $\mathcal{S}(\mathbf{x}, t)$ contains effects corresponding to the unsteady volume and momentum exchange between the body and the fluid, represented by distributions of monopole and dipole sources on the body surface, and to the unsteady fluid stress, represented by the Lighthill (1952, 1954) quadrupole sources distributed throughout the fluid. This equation has been applied with extraordinary regularity and success, but from the point of view of high-frequency asymptotics it is not completely satisfactory. Essentially, the effects that are most commonly studied in high-frequency asymptotics, such as refraction through the non-uniform flow or diffraction by sharp edges, are present but only in a heavily

disguised form within the source term \mathcal{S} . An alternative formulation, which is provided by Goldstein's (1978) version of rapid distortion theory (RDT), is therefore adopted here. The unsteady flow is taken to be a linear perturbation to an irrotational mean base flow (but see §5 for a discussion of the effects of mean vorticity). By decomposing the unsteady fluid-velocity perturbation in the form $\mathbf{v}' + \nabla G$, where \mathbf{v}' is the so-called vortical velocity (since the unsteady vorticity is given purely as $\nabla \times \mathbf{v}'$), an alternative to (1.1) is written by Goldstein as

$$\frac{D_0}{Dt} \left(\frac{1}{c_0^2} \frac{D_0 G}{Dt} \right) - \frac{1}{\rho_0} \nabla \cdot (\rho_0 \nabla G) = \frac{1}{\rho_0} \nabla \cdot (\rho_0 \mathbf{v}'), \quad (1.2)$$

where ρ_0 , c_0 are the steady (spatially non-uniform) density and sound speed, respectively, and D_0/Dt is the convective derivative with respect to the steady base flow. (An equation for \mathbf{v}' can also be derived, see (5.3).) One clear difference between (1.2) and (1.1) is that in (1.2) the non-uniform steady base flow is displayed explicitly within the wave operator on the left-hand side, rather than being implicitly included within the source term on the right-hand side of (1.1). This is a clear benefit of (1.2), because it means that the long-range refractive effects of non-uniform mean flow are accounted for by the wave operator and not by the source. The source region therefore only includes areas where new sound is actually being generated, and therefore becomes more localized in space. In fact, the source term is now confined to regions of space where $\rho_0 \mathbf{v}'$ is non-solenoidal, and we shall see that at high frequency this source region is small. A second difference is that (1.1) is in practice solved in free space, with the right-hand side treated as being known, while (1.2) must be solved subject to suitable boundary conditions on the body surface. The effects of wave diffraction can therefore be included within the Goldstein formulation using Keller's (1962) powerful geometrical theory of diffraction, in which local regions of wave scattering are isolated at high frequency and treated using canonical solutions to model problems.

This paper is set out as follows. In §2 we describe the use of high-frequency asymptotics to determine the noise generated by the interaction between unsteady vorticity and a single aerofoil. This is extended to the case of a cascade of aerofoils, as being more representative of a blade row, in §3. In §4 the propagation of noise both through the engine duct and out to the far field, is considered. Some further topics and extensions are described in §5.

2. Noise generation by a single aerofoil

We wish to consider the noise generated by the interaction between unsteady disturbances and a stationary rigid aerofoil placed in an oncoming flow (figure 2a). The oncoming disturbance corresponds to an azimuthal harmonic of the wake shed from the fan, and the aerofoil is of course a cross-section of one of the stator blades. Here we are making a two-dimensional approximation, in considering the flow at a single radius, which is legitimate for the high frequencies we consider. The theory described in this section was developed in great detail by Myers & Kerschen (1995, 1997) and Tsai (1992), and our aim here is to present a relatively concise discussion of their work.

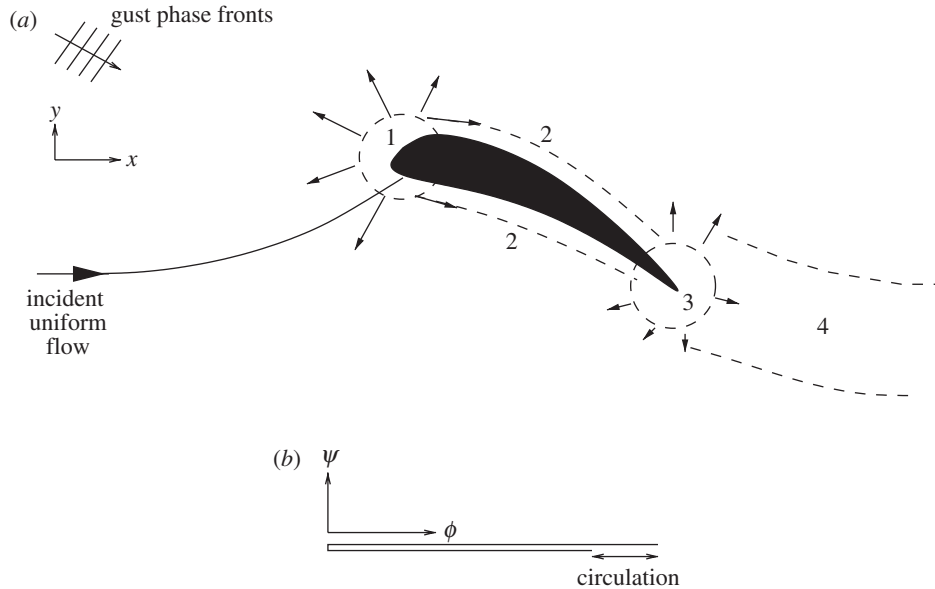


Figure 2. Schematic of high-frequency gust/aerofoil interaction. (a) Asymptotic regions in physical space: 1, leading-edge region; 2, surface-transition region; 3, trailing-edge region; 4, wake-transition region. (b) Image of aerofoil in (ϕ, ψ) -space.

(a) Problem formulation

We will see that the aerofoil geometry will play a crucial role in the noise generation. The upper and lower surfaces are described by the equations $y = \delta N^\pm(x)$, respectively, where the x -axis is aligned with the (uniform) mean flow at upstream infinity. We consider thin aerofoils, so that $\delta \ll 1$, and for simplicity suppose that the aerofoil has an infinite span in the radial (denoted here by z) direction, so that the steady flow is two dimensional. The aerofoil thickness, camber and angle-of-attack (or mean loading) are all contained within the shape functions $N^\pm(x)$. In some cases, $N^\pm(x)$ are known analytically (for instance, for NACA four-digit aerofoils, see Abbott & von Doenhoff (1959)). In other cases, closed-form expressions for $N^\pm(x)$ may not be available, but suitable spline interpolations of discretely defined surface points can easily be used for determining the steady flow. In the latter case, particular care would have to be taken to fit a parabola of the correct curvature in the nose region. In either case, the mean flow past the aerofoil is non-uniform, but can be calculated easily via thin-aerofoil theory, and it proves very convenient to use this mean flow to provide an alternative coordinate system. Specifically, we introduce as coordinates the mean flow potential ϕ and stream function ψ , and in (ϕ, ψ) -space the aerofoil is then mapped onto a single straight line (figure 2b). This has a number of advantages, including the way that the high-frequency scattering and diffraction problems for the thick aerofoil are mapped onto the equivalent canonical for a sharp, straight edge. There are drawbacks, however, including the fact that, at least for an aerofoil with non-zero lift (and hence non-zero circulation), the upper and lower sides of the trailing edge in physical space are mapped to *different* points in (ϕ, ψ) -space, and care must be taken when we come to treat the trailing-edge diffraction.

Noise is generated when the aerofoil and the flow close to it interact with the incident unsteady vortical disturbances generated upstream by the fan. Consider just a single harmonic component, or gust, of some more complicated incident disturbance. The disturbance will have a small amplitude, $O(\epsilon)$ say, in order to allow linearization about the steady base flow. The gust is convected and distorted by the non-uniform base flow, and Goldstein (1978) has shown how RDT can be used to describe the distorted gust throughout the flow, in terms of its form upstream. In (ϕ, ψ) -coordinates Kerschen & Balsa (1981) have shown that the associated unsteady vortical velocity is

$$\mathbf{v}' = \epsilon U_\infty (\tilde{A}_t, \tilde{A}_n, \tilde{A}_z) \exp(ik[\phi + k_n\psi + g + k_z z]). \tag{2.1}$$

Here U_∞ is the far-upstream mean flow speed, the subscripts ‘t’ and ‘n’ refer to directions parallel and normal to the local steady flow, and

$$g(\phi, \psi) = \int_{-\infty}^{\phi} \left[\frac{U_\infty^2}{|\mathbf{U}|^2(\xi, \psi)} - 1 \right] d\xi \tag{2.2}$$

is Lighthill’s (1956) drift function describing the cumulative distortion of vortex lines approaching the aerofoil, where $|\mathbf{U}|$ is the local mean-flow speed. One crucial parameter in (2.1) is k , the aerodynamic reduced frequency defined by

$$k = \frac{\omega b}{U_\infty}, \tag{2.3}$$

with ω the temporal gust frequency and b the aerofoil semi-chord. We suppose throughout that $k \gg 1$, so that in the usual Wentzel–Kramers–Brillouin (WKB) terminology (see Hinch 1991, p. 127) the gust possesses a rapid phase, while the amplitudes $(\tilde{A}_t, \tilde{A}_n, \tilde{A}_z)$ vary on the slow scale of the mean flow. The wavenumbers k_n and k_z correspond to the streamline-normal and spanwise directions, and are imposed at upstream infinity. In equation (2.1), and elsewhere, a time-harmonic factor $\exp(-ikt)$ has been suppressed.

A small simplification can be obtained by considering the modified unsteady velocity potential, $h(\phi, \psi)$, instead of the full unsteady velocity potential $G(\phi, \psi)$ (h contains extra factors (see Peake & Kerschen 1997), which have the effect of transforming out terms in the linear wave equation arising from the uniform mean flow at upstream infinity). The wave equation (1.2) then takes the form

$$\mathcal{L}_0 h + \delta \mathcal{L}_1 h = k \delta S(\phi, \psi) \exp(ik\Omega). \tag{2.4}$$

The operator \mathcal{L}_0 is simply the Helmholtz operator in (ϕ, ψ) -space, and the frequency which appears in \mathcal{L}_0 is the (acoustic) reduced frequency kw , with

$$w^2 = \left(\frac{M_\infty}{\beta_\infty^2} \right)^2 - \left(\frac{k_z}{\beta_\infty} \right)^2, \tag{2.5}$$

M_∞ is the (subsonic) upstream Mach number and $\beta_\infty^2 = 1 - M_\infty^2$. Strictly speaking, our analysis will require $kw \gg 1$ (specifically, *inter alia*, to allow the aerofoil leading and trailing edges to be considered separately). This condition will usually be achieved if $k \gg 1$, but perhaps significantly it is violated for very oblique high-frequency gusts for which k_z is large. In (2.4) the operator \mathcal{L}_1 is a second-order linear operator with spatially varying coefficients, which accounts for the refraction of the

sound as it propagates through the non-uniform steady flow (again recall that in (1.1) this effect is included on the right-hand side). On the right of (2.4) the source term $S(\phi, \psi) \exp(ik\Omega(\phi, \psi))$ arises from the interaction between the steady flow and the vortical gust. Full expressions for \mathcal{L}_1 , $S(\phi, \psi)$ and $\Omega(\phi, \psi)$ are given in Myers & Kerschen (1995, 1997).

(b) *Asymptotic solution near the leading edge*

Equation (2.4) must now be solved, subject to the boundary conditions of zero total normal velocity on the aerofoil surface $\psi = 0$, continuity of unsteady pressure in the fluid and outgoing acoustic waves at infinity. Numerical solution is certainly possible, and the reader is referred to the work of Atassi and co-workers (e.g. Atassi *et al.* 1990; Scott & Atassi 1995) for full details. However, here we describe the use of high-frequency ($k \gg 1$), thin-aerofoil ($\delta \ll 1$) asymptotics. The preferred limit $k\delta = O(1)$ is chosen, which corresponds to the case in which the gust wavelength is comparable with the blade thickness but is much shorter than the blade chord.

Throughout, we will be seeking solutions of (2.4) with phase $O(kw)$, and it therefore follows that in most of the flow the source term on the right-hand side of (2.4) does not appear to leading order (i.e. to $O(kw)^2$). However, close to the leading edge the steady fluid velocity has the characteristic thin-aerofoil $r^{-1/2}$ singularity (r, θ are polar coordinates in (ϕ, ψ) -space with the origin at the leading edge). This singularity appears in the source term, so that in the *inner* region, defined to be of size $O(\delta)$ around the leading edge, with inner coordinates $(\Phi, \Psi) \equiv \delta(\phi, \psi) = O(1)$, the source term is promoted and noise is generated. The *outer* region is taken to be the rest of space outside the inner region.

At leading order in the inner region one simply solves the Helmholtz equation

$$\mathcal{L}_0 H_0 = 0, \quad (2.6)$$

subject to zero total normal velocity on the semi-infinite domain $\Psi = 0, \Phi \geq 0$. Here, the incident gust is converted into nascent acoustic waves by the usual process of unsteady momentum blocking by the rigid blade, and the solution is completed in a familiar way via the Wiener–Hopf technique (Noble 1988). The next order in the asymptotic expansion of the unsteady potential is $O(\delta k^{1/2})$ smaller than the leading order, thanks to the inverse-square-root singularity in the steady flow, and much richer behaviour occurs, as follows.

- (i) A term H_1 arises from the fact that the gust is distorted as it propagates towards the leading edge in the inner region, with the effect that its upwash on the blade surface is slightly different from the upwash used in calculating H_0 . We have that H_1 again satisfies (2.6), but $\partial H_1 / \partial \Psi$ on $\Psi = 0$ must be chosen to satisfy the condition of zero total normal velocity on the genuine blade surface. This means that H_1 accounts for local vorticity distortion in the inner region.
- (ii) A term H_2 is generated by the volume source term, and satisfies

$$\mathcal{L}_0 H_2 = S(\Phi, \Psi) \exp(i\Omega(\Phi, \Psi)). \quad (2.7)$$

This source term is entirely analogous to the Lighthill quadrupole source: the Lighthill term contains the Reynolds stress formed from the total velocity, and the source term here is simply the linearized version of that, in which the unsteady vortical velocity is crossed with the local mean flow.

- (iii) A term H_3 is required finally to account for the effects of the non-uniform flow operator \mathcal{L}_1 in the local leading-edge region. Expanding the variable coefficients in \mathcal{L}_1 , it can be seen that H_3 again satisfies an inhomogeneous Helmholtz equation but, unlike in (2.7), the source term is now forced by H_0 , the leading-order acoustic field, rather than by the incident gust. In contrast to conventional ray acoustics, the interaction between H_0 and the local mean flow in the inner region occurs on the wavelength-scale (recall $k\delta = O(1)$). This causes additional noise to be generated, which corresponds to H_3 .

Full details of steps (i)–(iii) above can be found in Myers & Kerschen (1995). The total unsteady velocity potential in the inner region is now of the form

$$H_0 + \delta k^{1/2}(H_1 + H_2 + H_3),$$

and in order to match this with the field in the outer region the outer limit of this inner solution is required. In fact, it turns out that the outer limit of each term takes the form

$$D_i(\theta) \frac{\exp(ikwr)}{r^{1/2}}$$

for $i = 0, 1, 2, 3$, where expressions for the directivity functions D_i have been derived. $D_0(\theta)$ possesses the cardioid $\sin \frac{1}{2}\theta$ -dependence characteristic of a non-compact edge dipole, but the remaining terms are significantly more complicated, and the total directivity then represents the interference between all the physical effects described above.

(c) *Outer solution*

We now turn our attention to the outer region away from the leading edge. We have already indicated that we seek ray solutions with a fast phase, and by substituting the unsteady potential in the form

$$A(r, \theta) \exp(ikw\sigma) \tag{2.8}$$

into (2.4), the eikonal and transport equations are found at $O(kw)^2$ and $O(kw)$, respectively. Expanding the eikonal in powers of δ shows that the phase takes the form $\sigma = r + \delta p(\theta) + \dots$, where $\delta p(\theta)$ is found in closed form as a radial integral of the non-uniform local perturbation to uniform mean flow (hence the factor δ). To leading order in δ , the transport equation can be solved with amplitude corresponding to the cylindrically decaying field of a point source of arbitrary directivity located at the origin. The final step to determine this directivity can then be made by matching the outer field to the outer limit of the inner solution. In fact, putting all this together, we end up with an acoustic unsteady potential, $h_1(r, \theta)$ say, emanating from the leading-edge region and of the form

$$h_1 = k^{-3/2} r^{-1/2} [D_0 + \delta k^{1/2}(D_1 + D_2 + D_3)] \exp(ikwr + ikw\delta p(\theta)). \tag{2.9}$$

Note here that the effects of the blade camber, thickness and mean loading are manifested in a number of places. The total directivity is that of a simple flat plate, $D_0(\theta)$, with an $O(\delta k^{1/2})$ correction which, while formally small, could be important in practice. More significantly, the phase function has an $O(k\delta) = O(1)$ correction, and in the next section this will be crucial because we will be considering the interference

between fields from multiple aerofoils. Further, equation (2.9) is expressed in terms of polar coordinates in (ϕ, ψ) -space, which themselves depend on the non-uniform flow. Far upstream, ϕ and ψ approach the physical Prandtl–Glauert coordinates x and $\beta_\infty y$, respectively, but in the near field the two sets differ by a non-zero, but $O(\delta)$, amount.

The noise from the leading edge will propagate directly to the far field, and will also interact with the rest of the aerofoil away from the leading-edge region. For the high frequencies considered, the leading-order re-scattered field will come from the trailing edge region, with corresponding modified potential $h_t(\phi, \psi)$. The asymptotic structure required to describe this is quite subtle, but the regions of interest are set out in figure 2*a*. For a cambered aerofoil, there is a transition region of width $O(1/k)^{1/2}$ along upper and lower surfaces, describing the propagation of the two rays from the leading edge in the directions $\theta = 0, 2\pi$, i.e. at grazing incidence to the aerofoil surface. This transitional field is then scattered by the trailing edge. The mechanism for scattering is simply that the downstream-propagating unsteady pressure jump across the aerofoil cannot be supported across the wake downstream of the trailing edge, and a cylindrically decaying acoustic field emanating from the trailing edge is therefore produced to cancel this pressure jump. Thanks to the Kutta condition, the steady flow around the trailing edge is much smoother than that found at the leading edge, so that no flow sources are present here. The scattered field is then essentially the same as that produced by the scattering of a plane wave by a sharp edge, with one important distinction. As already noted, the trailing edge is mapped onto two points in (ϕ, ψ) -space, and in order to handle this mathematically it is necessary to introduce *trailing-edge* coordinates, (ϕ_t, ψ_t) , which are discontinuous in such a way that the trailing edge lies at a single point, the origin, in (ϕ_t, ψ_t) -space. (This is equivalent to moving the steady-flow branch point from the leading edge to the trailing edge). The scattered field then has a directivity which is proportional to $1/\sin \frac{1}{2}\theta_t$, which is itself singular along the wake direction $\theta_t = 0$, due to the geometric acoustics approximation breaking down along a shadow boundary. This singularity is made finite by the introduction of a wake transition region (see figure 2*b*), again of width $O(1/k)^{1/2}$, in which inclusion of the fact that the two rays from the leading edge have a cylindrically decaying amplitude renders the transition solution finite.

The trailing-edge scattered potential h_t is $O(1/k^{1/2})$ smaller than the leading-edge field h_l , as is typical in high-frequency diffraction problems, and the total acoustic field is simply $h_l + h_t$. Finally, a hydrodynamic field $h_p(\phi, \psi)$ is also included to enforce the normal velocity boundary condition as the incident gust propagates along the blade surface. Since the gust propagates subsonically, however, h_p decays exponentially away from the blade surface, and is therefore analogous to a cut-off sound wave which need not be included in the far field.

A sample far-field directivity is shown in figure 3. Note how the sound is significantly enhanced below the horizontal, thanks to the effects of the camber and (nose-up) angle of attack. The lobular nature of the directivity is a result of interference effects between the leading- and trailing-edge fields, which individually have cardioid directivities to leading order but which interfere thanks to the phase distortion along the surface transition region and the distortion and path-length differences in propagating to the far field. The peak level is increased by *ca.* 20% compared with

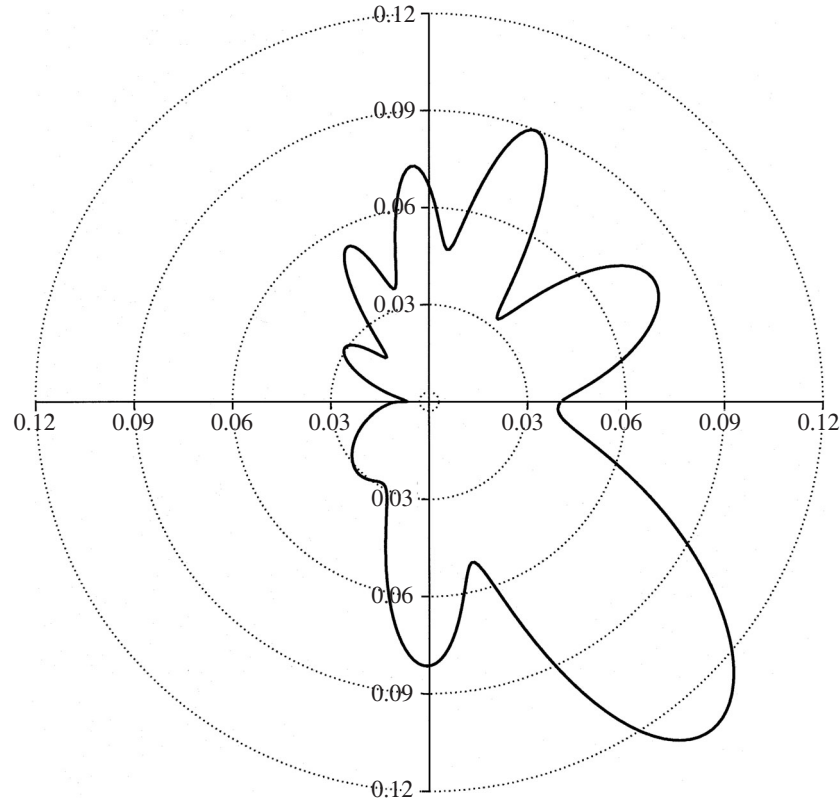


Figure 3. Far-field directivity for an aerofoil with zero thickness, at an angle of attack of 12° and maximum camber at 33% of its chord, with $M_\infty = 0.5$, $k = 8$. Flow is from left to right. (Reproduced with permission from Myers & Kerschen (1997). Copyright © Cambridge University Press.)

a purely flat-plate result. We can therefore see that the aerofoil geometry is having a significant effect on the radiated noise.

3. Noise generation by a cascade

In turbo machinery, blades are placed in close proximity to each other, and mutual aerodynamic interactions are sufficiently strong to invalidate the use of the sort of single-aerofoil model described in §2. Much progress can be made along the same lines, however, by judicious summation of the main results from the previous section. Full details of the material described in this section are given in a series of papers by Peake (1992) and Peake & Kerschen (1995, 1997, 2004).

(a) Upstream radiation

Consider an infinite cascade of identical blades, with non-zero thickness, camber and angle of attack. Again we use (ϕ, ψ) -space, in which the cascade of real aerofoils becomes a cascade of flat plates, say with leading-edge separations Δ and stagger α (figure 4). The incident gust will strike each leading edge, generating cylindrically

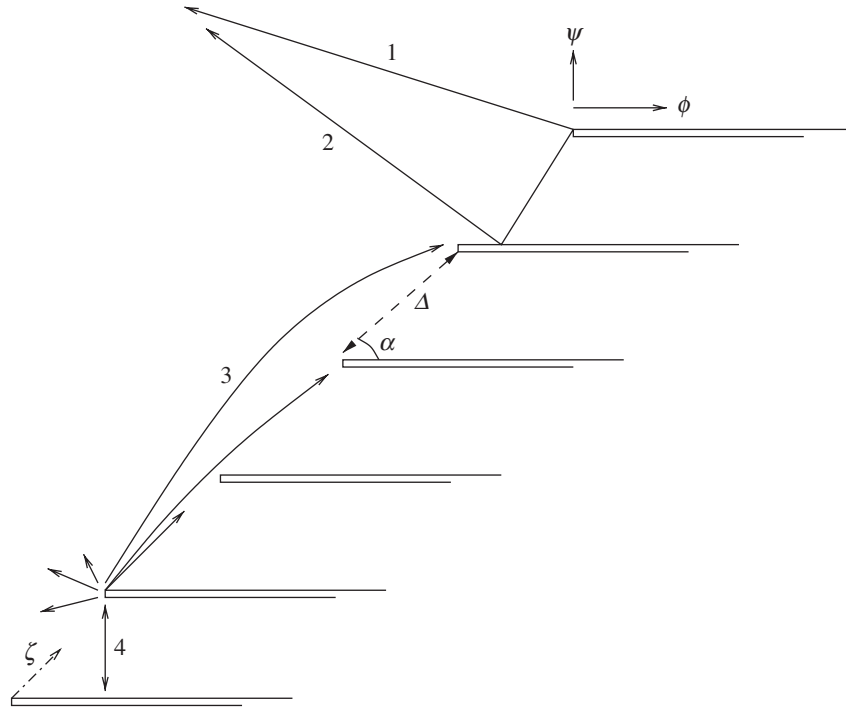


Figure 4. The cascade in (ϕ, ψ) -space. The numbered rays correspond to: 1, the direct field; 2, the reflected field; 3, the grating field; 4, the multiply reflected field.

decaying sound fields, and leading to a total ‘direct’ upstream field of the form

$$h \sim \sum_{n=-\infty}^{\infty} \frac{D(\theta_n)}{r_n^{1/2}} \exp(ikwr_n + ikw\delta p(\theta_n) + in\sigma'), \quad (3.1)$$

where now r_n, θ_n are polar coordinates in (ϕ, ψ) -space centred on the leading edge of blade n . The quantity σ' arises from the transverse phasing of the gust between adjacent leading edges.

The sound field upstream of a cascade differs from that upstream of a single aerofoil, in that the former is made up of a superposition of plane waves, rather than being a cylindrically decaying field. To see this in (3.1), first note that the series can be converted into a series of delta functions by introducing an integral in the ζ -direction (figure 4) along the front face of the cascade, with integrand containing terms $\delta(\zeta - n\Delta)$. Poisson’s summation formula is then applied to convert the series of delta functions into a series of complex exponentials and, after a series of manipulations, including taking the far-field limit, one arrives at the result

$$h \sim \sum_{m=r}^q A_m \exp[ik(wr \cos(\theta - \theta_s^m) + \delta p(\theta_s^m))]. \quad (3.2)$$

The discrete angles θ_s^m are the propagation angles of the plane waves, and satisfy

$$\cos(\theta_s^m - \alpha) = \frac{\sigma' - 2n\pi}{\Delta kw}.$$

The integers m satisfying $r \leq m \leq q$ in the summation (3.2) form the range over which $\alpha < \theta_s^m < \pi + \alpha$, i.e. for which the plane waves propagate ahead of the front face of the cascade. For integers m outside this range, the plane-wave modes are cut-off and do not propagate upstream. The modal amplitudes A_m can be determined, and contain a leading term corresponding to the flat-plate cascade plus a small, $O(k\delta^{1/2})$, correction due to the non-uniform mean flow. However, the effect of non-uniform flow on the phase terms turns out to be more significant.

The direct field of rays from each leading edge (figure 4, ray paths labelled ‘1’) is supplemented by the reflection of these fields from adjacent blades (figure 4, ray paths labelled ‘2’). A far-field observer at an angle θ with $\frac{1}{2}\pi < \theta < \pi - \alpha$ will receive a reflected field, and this reflected field is of course described by an image source in the corresponding blade. The image-source contribution must then be included in (3.2), which leads to the direct-field amplitude A_m being multiplied by the factor

$$1 - \exp(2ikw\Delta \sin \alpha \sin \theta_s^m + ik\delta p_3(\theta_s^m)). \quad (3.3)$$

The second term in (3.3) corresponds to the contribution from the image source, and the difference in phase between the direct and image fields arises from both the familiar difference in path length (approximated as $2\Delta \sin \alpha \sin \theta_s^m$), and the fact that the distortion due to the non-uniform mean flow differs between the direct and reflected paths. This latter effect is expressed by the term $k\delta p_3(\theta_s^m)$, and we recall that $k\delta = O(1)$.

Equation (3.3) makes it clear that the non-uniform flow will have a significant effect on cascade noise. For instance, note that the amplitude of a given mode will become zero when the mode propagates in certain discrete directions, corresponding to cases in which there is total destructive interference between the direct source and the image and the factor (3.3) becomes zero. Conversely, in other preferred modal directions there is total constructive interference between the direct and image sources, and the modal amplitude is doubled. The effect of the non-uniform mean flow, through the term $k\delta p_3(\theta_s^m)$ in (3.3), is to change the phase along the reflected ray by an $O(1)$ amount, and therefore completely change the interference between the two sources. Indeed, if $k\delta p_3(\theta_s^m) > \pi$, then there is the possibility of what would have been a total destructive interference for a given mode in uniform mean flow becoming total constructive interference once non-uniform flow effects are included, and vice versa.

The direct and reflected fields mentioned above do not account for all the radiation which reaches an observer upstream, because these fields can themselves be multiply re-scattered by the other blades to yield additional contributions which are $O(k^{-1/2})$ smaller than those already described. For instance, the direct field from any given leading edge will propagate along the front face of the cascade as a grating mode (figure 4, contribution ‘3’), being re-scattered by each edge as it goes. According to a result due to Macdonald (see Goldstein 1976, p. 175), if a source and an observer are placed equidistant from the sharp edge of a rigid semi-infinite plate, with the line of sight between the source and the observer passing exactly through the edge, then the sound received by the observer is half what would have been measured if the plate had been absent. For high frequencies this result has been generalized to the cascade case by Lee (1978), who shows that, if $n - 1$ plates lie between the source and the observer, then to leading order the sound is reduced by a factor $1/n$. When combined with the cylindrical spreading, this effect means that the field from a given leading

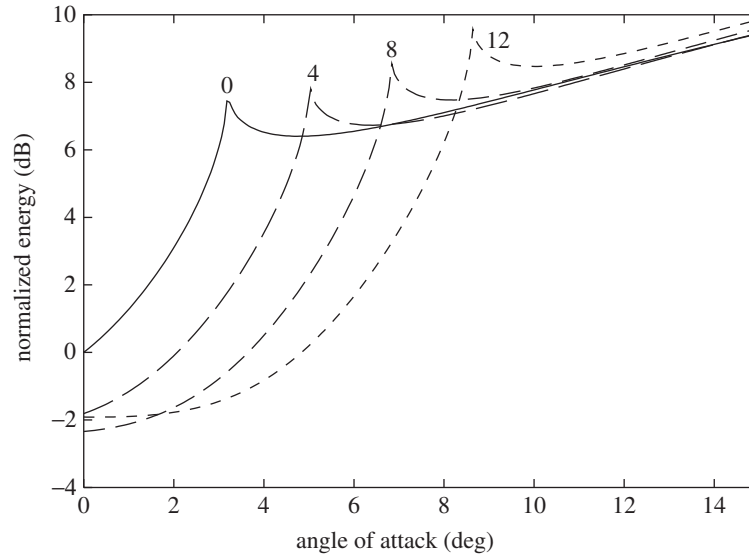


Figure 5. Plot of the change in the upstream acoustic energy flux. The cascade consists of uncambered NACA00XX blades at varying angles of attack, with $M_\infty = 0.5$. The XX refers to the maximum thickness-chord ratio, and aerofoils with 0% (flat plate), 4, 8, 12% thicknesses are plotted. The decibel change is measured relative to the datum case of a flat plate at zero angle of attack. (Reproduced with permission from Evers & Peake (2002).)

edge will decay like $1/n^{3/2}$, before being re-scattered at the n th edge en route to the far field. In a similar way, rays can be repeatedly reflected between a given leading edge and the neighbouring blade (figure 4, contribution '4'), being re-scattered by the edge on each occasion. Both these sorts of contributions can then be included in the asymptotic prediction of the upstream noise, and full details are given in Evers & Peake (2002). A sample result for the total upstream acoustic energy (i.e. summed over all cut-on modes) is given in figure 5, where it becomes clear that the non-uniform flow is indeed having a significant effect, even on a decibel scale. As already discussed, this can only be due to the way in which the non-uniform flow changes the interference between the different acoustic sources.

(b) Downstream radiation

The noise generated at the cascade leading edges will also propagate downstream in the blade passages, and a modal expansion for the multiply reflected rays can be derived. These modes are entirely analogous to the familiar modes in a two-dimensional straight duct with uniform (or zero) flow, but once again our non-uniform flow introduces $O(1)$ phase distortions. Only a finite number of the duct modes will propagate, at discrete angles χ_n which depend on both the cascade geometry and on the non-uniform flow. In ray terms the duct modes are made up of an upwards travelling and a downwards travelling ray, both at an angle χ_n to the blades, and which are repeatedly reflected between the blades. Once the duct modes reach the blade trailing edges they are re-scattered, exactly as described in §2 for a single aerofoil, to produce radiation downstream of the cascade. In practical terms, this radiation corresponds to the noise radiated into the bypass duct downstream of the

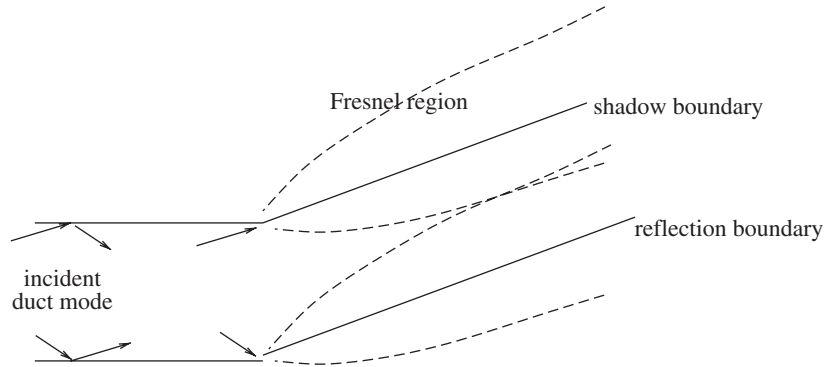


Figure 6. Schematic, in (ϕ_t, ψ_t) -space, of the interaction between the scattered fields from adjacent trailing edges. The acoustic far-field is reached once the Fresnel regions have merged. Boundaries of Fresnel regions are denoted by dotted lines.

stator (see figure 1). Just as upstream, the acoustic field downstream of the cascade is modal, but the process by which these modes are formed is quite different to what happens upstream, and is worth further discussion.

We again adopt downstream potential-stream function coordinates, $\phi_t - \psi_t$, which render the mapping from physical space single-valued at the trailing edge. For simplicity, suppose now that the cascade has zero stagger, $\alpha \rightarrow \pi/2$, in this space (non-zero stagger can easily be included but complicates the discussion), and consider a single duct mode with mode angle χ in the passage. The high-frequency limit of the scattered field from any trailing edge is then proportional to

$$\frac{\cos(\frac{1}{2}\chi) \sin(\frac{1}{2}\theta_t)}{\cos \chi - \cos \theta_t} \exp(ikwr + ik\delta p(\theta_t)), \tag{3.4}$$

where now polar coordinates r_t, θ_t are measured relative to that edge, and again the factor $p(\theta_t)$ accounts for the mean-flow distortion. When considering the radiation emanating from a given blade passage, one must add the scattered field from two trailing edges (see figure 6). For an observer in the far field, both these fields are (individually) singular along the shadow and reflection boundaries $\theta_t = \pm\chi$, thanks to (3.4). However, when added together the singularity in the reflected field from the upper trailing edge cancels with the singularity in the shadow boundary from the lower trailing edge, and vice versa. In fact, what happens mathematically is that the phase difference between the duct-mode rays hitting the lower and upper trailing edges combines with the differing path lengths on the rays from each edge to a given observer to produce total destructive interference, and therefore zeros in the numerator, along $\theta_t = \pm\chi$. These zeros cancel the corresponding zeros in the denominator of (3.4). The resulting directivity is non-singular, and possesses two strong beams which, for uniform flow, lie along $\theta_t = \pm\chi$. The effect of non-uniform flow is simply to tilt the direction of these beams by a small amount (in fact, by an angle $O(\delta)$). This sort of effect is very familiar in problems of diffraction by finite bodies; the individual scattered fields from each edge possess narrow Fresnel regions which spread downstream, and at sufficient distance eventually intersect. Beyond the so-called Rayleigh distance, of size $O(kw\Delta^2 \cos^2 \chi)$, these regions have merged and the genuine acoustic far field is obtained. Then, the expected plane-wave modes

can be obtained by adding together all such far fields from each blade passage, and we now see that, if one of those modes happens to be propagating along a direction parallel to one of the duct modes in the blade passages, then that mode will have a particularly large amplitude, thanks to the beaming effect described above. What might also happen, however, is that this far-field behaviour is never reached—the Rayleigh distance increases with k , and at high frequency it is possible that there is some downstream obstacle lying within the Rayleigh distance (perhaps a structural support in the bypass duct). In such a case the noise striking the obstacle will still be modal, but would now be better thought of as being composed of the sum of the geometrical acoustics field which travel straight out of each blade passage without being scattered by the trailing edges.

4. Duct acoustics

In the previous two sections we have been concerned with one way in which noise can be generated within the engine, but we will now consider how that noise will propagate along the engine nacelle, and how the noise escapes through the inlet to an observer in the far field. The geometry of such a real engineering problem is clearly exceedingly complicated, but considerable insight can be derived from consideration of highly simplified model problems.

(a) Axisymmetric problem

Consider first a straight cylindrical duct of radius a . Ignoring all mean-flow effects, single-frequency acoustic disturbances satisfy the Helmholtz equation $(\nabla^2 + k_0^2)p = 0$, where p is the acoustic pressure, $k_0 = \omega/c_0$, ω is the frequency and c_0 the speed of sound. Rigid walls are assumed in the first instance. It is very well known that the acoustic field possesses eigensolutions of the form

$$p_{mn} = J_m\left(\frac{j'_{mn}r}{a}\right) \exp(im\varphi + ik_x x) \quad (4.1)$$

for all integers m, n with $n \geq 1$, where (r, φ, x) are cylindrical polar coordinates, j'_{mn} is the n th zero of $J'_m(z)$ and the axial wavenumber is

$$k_x = \sqrt{k_0^2 - \left(\frac{j'_{mn}}{a}\right)^2}.$$

A high-frequency analysis of this eigenmode has been completed by Chapman (1994), using the large-argument, large-order expansion of the Bessel function; specifically, for $r > r_{mn} \equiv am/j'_{mn}$ he writes p_{mn} in the form

$$p_{mn} \sim \left(\frac{2r_{mn}}{m\pi\sqrt{r^2 - r_{mn}^2}}\right)^{1/2} \exp(im\varphi + ik_0 x \cos \theta_{mn}) \cos(m \tan \eta - m\eta - \frac{1}{4}\pi), \quad (4.2)$$

where

$$\sin \theta_{mn} = \frac{j'_{mn}}{k_0 a}, \quad \sec \eta = \frac{r}{r_{mn}}.$$

The form of equation (4.2) allows Chapman to identify the ray structure of the duct mode. The radius $r = r_{mn}$ is a caustic cylinder on which the outer expansion (4.2)

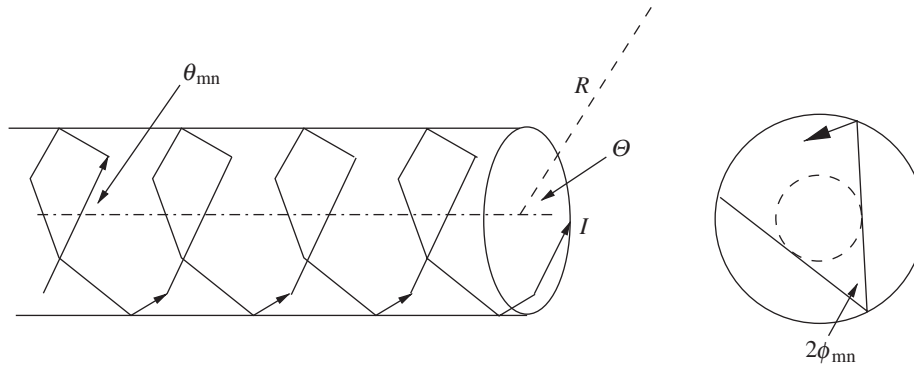


Figure 7. Diagram of Chapman’s piecewise linear helix, side view and front view. The angle θ_{mn} is the angle between each ray and the cylinder axis, while $2\phi_{mn}$ is the angle between rays projected into the plane perpendicular to the axis. The dotted circle is the caustic cylinder $r = r_{mn}$. The polar angle, Θ , and the distance of the observer from the centre of the open end, R , are also shown.

is singular, with quiet zone inside, and with two rays passing through each point outside; note the $\frac{1}{4}\pi$ term in the argument of the cosine in (4.2) guarantees the usual $\pi/2$ phase shift between rays entering and leaving the caustic. The rays themselves lie on planes which are tangent to the caustic cylinder—the ray makes an angle θ_{mn} with the x -axis in this plane, as is made clear by the fact that the x wavenumber in (4.2) is $k_0 \cos \theta_{mn}$. At the cylinder wall one (outward-going) ray in (4.2) is simply reflected into the other (inward-going) ray, and there is an angle $2\phi_{mn}$ between the planes containing these two rays. Via simple geometry it follows that

$$\sin \phi_{mn} = \frac{m}{k_0 a \sin \theta_{mn}} = \frac{m}{j'_{mn}}. \tag{4.3}$$

Chapman thereby shows how the duct eigenmode can be viewed as rays forming a piecewise linear helix in $r_{mn} \leq r \leq a$, which is completely described by the two angles θ_{mn} and ϕ_{mn} (see figure 7).

Having found the ray structure of the propagating mode within the duct, one is in a good position to consider the way in which that mode is scattered when it reaches the open end of the duct. The use of Keller’s (1962) geometrical theory of diffraction (GTD) is suggested by Chapman (1994) for a cylindrical duct with an axisymmetric open end (i.e. open face orthogonal to the cylinder axis), and this approach has been successively developed by Chapman (1996), Hocter (2000) and Keith & Peake (2002a). According to GTD, the point where the duct-mode ray hits the edge of the cylinder, point I in figure 7, is the vertex of a cone of diffracted rays. The cone is formed by rotating the extended incident ray about the local tangent to the edge, i.e. in this axisymmetric case by rotating about the φ -direction, and the unsteady field on the cone is then found simply by applying the canonical diffraction coefficient, \mathcal{D} , for scattering of a plane wave by a straight edge. (Note that in this high-frequency limit the wavelength is much shorter than the cylinder radius, $ka \gg 1$, so that straight-edge scattering is appropriate.) The diffracted field then takes the form

$$\frac{A\mathcal{D}}{\sqrt{\Sigma j}} \exp(ik\Sigma), \tag{4.4}$$

where A is the complex amplitude on the incident ray at I , Σ is the distance of the observer from I and Σj is the Jacobian of the transformation that is effected from physical to ray coordinates in calculating (4.4). This calculation has been performed by Hocter (2000), and good agreement with an exact solution is found in regions where the GTD is valid.

Unfortunately, equation (4.4) fails in a number of directions, including in the direction of the principal lobe where the far-field sound is loudest, and uniform asymptotic calculations are required (Keith & Peake 2002a). First, there is a caustic surface, $j \rightarrow 0$, dividing an insonified region where each observer receives a diffracted ray from two Keller cones from a quiet region where no rays are received. In the far field the quiet zone lies inside the cone $\Theta = \arcsin(m/k_0a)$. The caustic singularity in GTD has been dealt with by Ludwig (1966) by postulating an inner expansion around the caustic which matches onto the GTD outer field. Second, the diffraction coefficient D depends on the angles made by the projection of the incident ray and observer–vertex directions into the radial plane through the cone vertex, and is singular when these two angles are equal (the shadow boundary) or the one is the negative of the other (the reflection boundary). In fact, the shadow and reflection boundaries correspond to directions along which the diffracted rays and rays from the geometrical acoustics field (i.e. the rays exiting straight out of the open-end of the duct) are collinear. What happens here is similar to what was described in § 3*b* for the cascade downstream radiation. The Fresnel regions around the shadow and reflections boundaries spread out and ‘eat’ into the geometrical acoustics field, and beyond the Rayleigh distance the Fresnel regions have overlapped to form a ‘Fraunhofer’ region. Unlike the cascade downstream radiation, the reflection-boundary singularities and shadow-boundary singularities do not cancel, and so we need uniform asymptotics to yield a finite result. In fact, Ludwig (1966) has presented uniform asymptotics for distinct shadow-boundary and reflection-boundary transitions, which were extended by Keith & Peake (2002a) to handle this overlapping case. The Rayleigh distance itself is $O(k_0a^2 \cos^2 \theta_{mn} \cos^2 \phi_{mn})$, which although formally large, since $k_0a \gg 1$, will in practice be more modest thanks to the two cosine squared factors.

In figure 8 we present a comparison between the uniform asymptotics (Keith & Peake 2002a) and the exact Wiener–Hopf solution (Weinstein 1969). The agreement is very pleasing indeed, for all observer angles. Note in particular how the principal lobe, at polar angle $\Theta \approx \theta_{mn}$, is resolved almost exactly. The asymptotics work well in both the near field and the far field. In this example the Rayleigh distance is $R \approx 5.6$, and we can see that the far-field behaviour is obtained very quickly beyond $R = 5.6$; in fact, the only real difference between the directivities for $R = 9$ and $R = 100$ is that in the latter the nulls have become more sharply defined. For the very far-field observer $R = 100$ in figure 8, the quiet zone is $0 < \Theta < 30^\circ$, the caustic region is $30^\circ < \Theta < 40^\circ$, there is then a very narrow GTD region, followed by the Fraunhofer region up to $\Theta \approx 60^\circ$, with finally a second GTD region for $\Theta > 60^\circ$. The discontinuity at $\Theta = 90^\circ$ corresponds to one of the GTD rays being intercepted by the duct wall, so that only a single ray reaches an observer for $\Theta > 90^\circ$ (a smooth approximation to cover this transition has not been derived).

(b) Scarfed cylinder

We will now move on to discuss, more briefly, the application of these ideas to a radical proposal for reducing aircraft environmental noise. The idea is to ‘scarf’ the

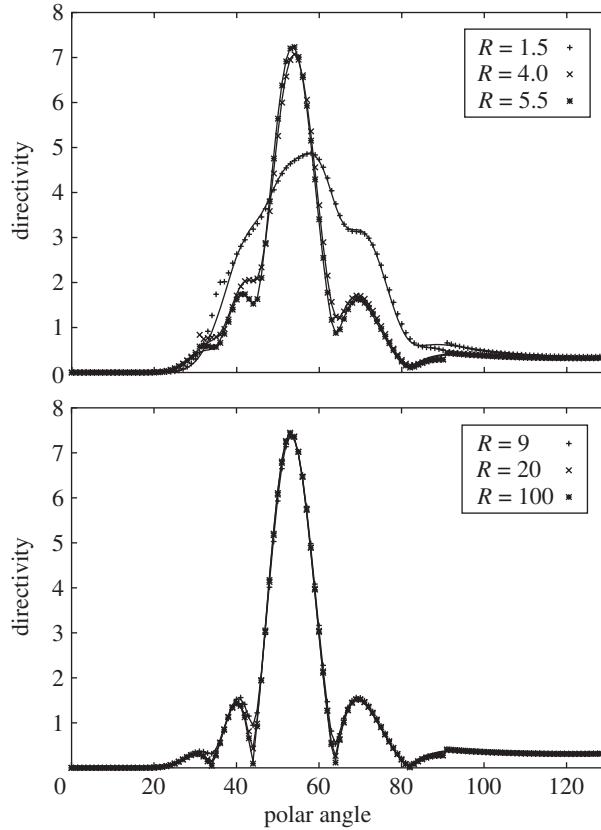


Figure 8. Amplitude of the acoustic pressure plotted against polar angle Θ ($\Theta = 0$ being on the axis dead ahead of the cylinder), for an incident duct mode of azimuthal order $m = 20$ and radial order $n = 3$ with $k_0 a = 40$. The symbols represent values calculated using the high-frequency asymptotics, while the solid lines represent exact values. The graphs are for different observer distances, R , normalized by the duct radius. (Reproduced with permission from Keith (2000).)

open end of the engine intake upwards so as to project more of the forward engine noise upwards away from ground detection microphone and away from the cabin. (The intake shown in figure 1 is scarfed slightly downwards, but what we mean by scarfing here is a much more significant asymmetry in the opposite direction.)

As a model of scarfing, we consider here again a semi-infinite hollow circular cylinder, but this time with its open end being a plane making an angle L with the cylinder axis (so that $L = 0$ reduces to the axisymmetric case considered already); see figure 9. Chapman’s ray description of the incident field within the duct still holds, of course, and the application of GTD and the uniform asymptotics across the caustics and shadow/reflection boundaries go through in exactly the same form as before (full details are given in Keith & Peake (2002b)). Results are shown in figure 9 for the power level, $P(\varphi)$, at fixed azimuthal angle φ , integrated over polar angle Θ , i.e.

$$P(\varphi) = \int_0^\pi |p(\Theta, \varphi)|^2 R^2 \sin \Theta \, d\Theta. \tag{4.5}$$

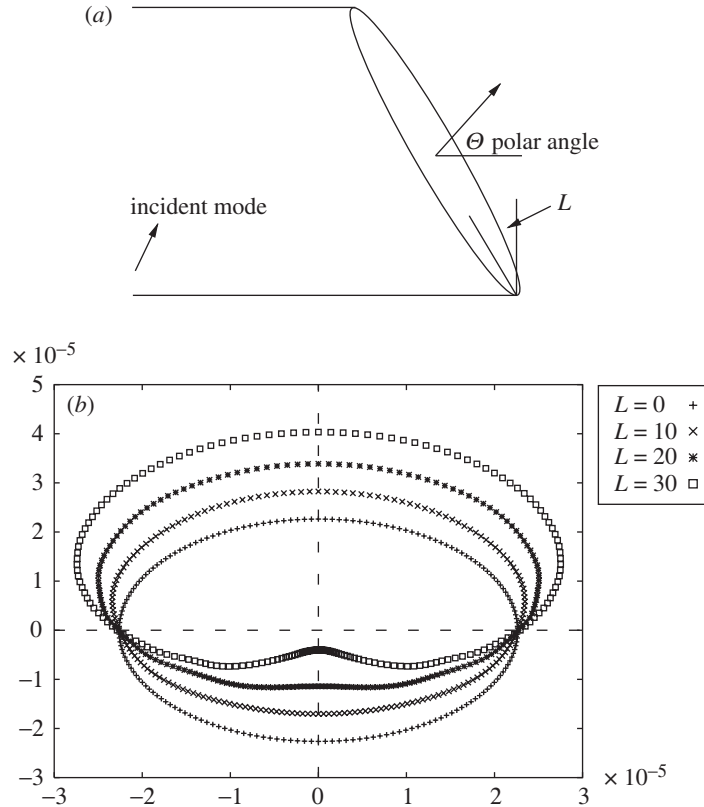


Figure 9. (a) Schematic of the model of the scarfed cylinder. (b) Asymptotic results for the integrated far-field power level, $P(\varphi)$, for the same duct mode as in figure 8. Scarfing angle L in degrees. What is shown in (b) is a polar plot of $P(\varphi)$ against φ , so that the horizontal and vertical coordinates are $P(\varphi) \cos \varphi$ and $P(\varphi) \sin \varphi$, respectively. (Reproduced with permission from Keith (2000).)

The effect of scarfing is to move the quiet zone and the caustic upwards towards the principal beam, which is then manifested in figure 9 by the upward distortion of the plots as L is increased. The *position* of the principal beam itself is determined by the duct mode (i.e. $\Theta \approx \theta_{mn}$), and is not affected by the scarfing, but of course its *amplitude* increases above the horizontal and decreases below. Another interesting feature, not readily apparent in the figure, is that the radiated field is not left–right symmetric, since the incident mode has rotational symmetry but the scarfed edge does not. We have restricted attention here to the case $\theta_{mn} < (\frac{1}{2}\pi) - L$. For larger values of θ_{mn} , corresponding to duct modes which are closer to cut-off, the effect of scarfing can be expected to be even more significant, since then the lower portion of the edge is not insonified and the quiet zone below the horizontal is extended.

5. Further topics

We will now proceed to describe extensions to some of the topics already presented.

(a) *Slowly varying duct*

The modal decomposition described in § 4a corresponds to a circular duct of uniform radius. However, in practice the cross-section of the engine nacelle varies along its length upstream and downstream of the spinner, as can be seen clearly in figure 1. The problem of absolutely general area variation is of course not amenable to analytical attack, but considerable progress can be made if one assumes that the duct varies *slowly* in the axial direction, and Rienstra (1999) has completed a particularly pleasing solution in this limit. He writes the duct inner and outer radii as $r = R_{1,2}(X)$, respectively, where $X = \epsilon x$ is a ‘slow’ axial coordinate, and $\epsilon \ll 1$ is the order of magnitude of the axial gradient of the walls. A consistent asymptotic solution for both the steady and unsteady flow is then obtained. The steady flow is one-dimensional plug flow to leading order, but with an $O(\epsilon)$ radial velocity induced by the area changed. The unsteady flow quantities are written in the generic WKB form with, for instance, the unsteady velocity potential (Rienstra 1999, eqn 4.2)

$$A(X, r) \exp\left(-im\varphi - i\epsilon^{-1} \int^X \mu(\xi) d\xi\right). \quad (5.1)$$

In the fast phase, $\mu(\xi)$ is the equivalent of the axial wavenumber k_x in (4.1) (note that μ also contains a Doppler term corresponding to the local axial flow, which is absent in the static case (4.1)). At leading order (5.1) satisfies the wave equation for locally parallel uniform axial flow, and it then follows that $A(X, r)$ must take the form (for simplicity here in the hollow case only)

$$N(X)J_m(\alpha(X)r), \quad (5.2)$$

where $\mu(X)$ and $\alpha(X)$ are related by the local dispersion relation. The quantity $\alpha(X)$ is then determined from the local wall boundary conditions, but at this order the envelope amplitude $N(X)$ is unknown. At the next order in ϵ , Rienstra finds a solvability condition, which gives an exact analytical expression for $N(X)$. The possibility of acoustic lining in the duct (see figure 1), modelled as impedance surfaces, is included in Rienstra’s solution. Comparison with careful numerics (Rienstra & Eversman 2001) shows that the asymptotics are exceedingly accurate, and in some cases, especially involving cut-off modes, do better than the numerics. Furthermore, impressive simulations have recently been completed by Zhang *et al.* (2003), in which the slowly varying duct theory has been seen to compare favourably with numerical solution of the full equations, in this case in the context of acoustic propagation along the bypass duct (see figure 1).

Rienstra’s discovery of a closed-form asymptotic solution is satisfactory, and the simplicity of his result has allowed a range of extensions, including the effects of mean swirl (Cooper & Peake 2001) and different cross-sectional shapes (elliptical pipes of slowly varying eccentricity (Peake & Cooper 2001), and now the general case (Rienstra 2003)) to be made.

(b) *Swirl*

In § 1 we described Goldstein’s (1978) version of the RDT for small disturbances to an irrotational mean flow, but we will now consider what happens when the mean

vorticity is non-zero. The wave equation (1.2) for the potential G is unaltered, while the equation for the vortical velocity \mathbf{v}' is

$$\frac{D\mathbf{v}'}{Dt} + (\mathbf{v}' \cdot \nabla)\mathbf{U} = -\boldsymbol{\xi} \times \nabla G, \quad (5.3)$$

where now $\boldsymbol{\xi} = \nabla \times \mathbf{U}$ is the mean vorticity and \mathbf{U} is the mean velocity. What is clear straight away is that in the irrotational-mean case the vortical velocity is decoupled from the unsteady potential, allowing \mathbf{v}' to be determined throughout the fluid, as stated in equation (2.1). However, when $\boldsymbol{\xi} \neq \mathbf{0}$ we see that equations (5.3) and (1.2) are fully coupled, so that they must be solved together. In physical terms, this arises because the acoustic velocity ∇G stretches the mean vorticity to produce extra unsteady vorticity, and leads to the term on the right-hand side of (5.3).

In the turbofan context there is significant mean swirl between the fan and the stator row, and it is therefore important to include this when attempting to understand the way that the fan wakes propagate downstream and sound waves propagate both upstream and downstream in the rotor–stator interstage gap. Kerrebrock (1977) was the first to consider this problem, and significant extensions have been made by Golubev & Atassi (1998) and Tam & Auriault (1998). In all cases it turns out that there are two quite distinct families of duct modes present: a ‘sonic’ family, entirely analogous to the ordinary acoustic modes of uniform flow, and a ‘nearly convected’ family. The latter modes all propagate downstream, at close to the convection speed of the base flow, and possess a non-zero but typically small pressure. In practice the modal decomposition of the flow is now very difficult, because this second family of modes often exhibits accumulation points and continuous spectra, making the computation of an adequate number of modes difficult. This has led Golubev & Atassi (2000) to propose the alternative approach of handling swirling flow, in which one essentially solves an initial-value problem for a given unsteady vortical and pressure distribution upstream, which propagates downstream and is distorted by the swirl. High-frequency asymptotics can again be used, however, and, for instance, Cooper & Peake (2001) have applied the WKB method to describe the evolution of unsteady swirling flow along a pipe of circular cross-section whose radius varies slowly along the axis, both steady and unsteady components being treated asymptotically. Of course, the WKB method can break down at turning points, or caustics, where the rays propagating down the duct turn round and a cut-on mode becomes cut-off, but an inner expansion can be made to provide a smooth transition through this region. In fact, in swirl this transition solution takes the well-known Airy-function form, and the wave incident on the caustic is reflected with a $\pi/2$ phase shift, exactly as in non-swirling flow.

(c) *Extensions of the blade response*

A number of open questions remain in the blade-response theory presented in §§2 and 3. For instance, note how the drift function (2.2) diverges (logarithmically) as the leading-edge stagnation point is approached. This issue has been addressed numerically by Atassi & Grzedzinski (1989); the total unsteady velocity is well-behaved near the stagnation point, and the singularity only appears in the decomposed components separately, so that Atassi & Grzedzinski are able to introduce an extra term to exactly cancel the singularity in ∇G . As far as our asymptotics are concerned,

this issue has not arisen because we have considered waves with a wavelength $O(\delta)$, whereas for a parabolic-nosed aerofoil the nose region is much smaller, of size $O(\delta^2)$, and the stagnation-point flow therefore has no effect on the leading-order term of our expansion. However, the effect would become important at higher orders, and also in the case of a more blunt aerofoil, for which the nose radius scales with δ rather than δ^2 . This issue certainly warrants further study.

Another possible extension concerns the case of a cascade of aerofoils with significant camber. One can expect that the sound generation is still confined to local leading-edge regions, and all that changes is that the steady flow can no longer be determined by thin-aerofoil theory. This would necessitate numerical ray tracing (e.g. Durbin 1983*a, b*) of sound as it propagates away from each leading edge, but such a calculation would be feasible, and the numerically sensitive parts of the flow, namely the sound generation regions, would still be modelled asymptotically. Work in this direction is continuing.

6. Concluding remark

It is hoped that this article has succeeded in its aim of showing that high-frequency asymptotic analysis can be used to provide important information, both qualitative and quantitative, about the aeroacoustics of a complicated engineering system. At present these high-frequency regimes present a formidable challenge to numerical computation, but in the future these engineering problems may well be solved routinely by accurate numerical solution of the full Navier–Stokes equations. However, the author believes that even then the asymptotic calculations will still play a valuable role, because of the very significant physical insights which they provide into the rich and many-faceted fluid mechanics of turbo machinery aeroacoustics.

Nomenclature

a	duct radius
A	ray amplitude (equation (2.8))
$\tilde{A}_{t,n,z}$	components of gust velocity
b	blade semi-chord
B	blade number
c_0	steady sound speed
\mathcal{D}	sharp-edge diffraction coefficient
D_i	directivity factors
G	unsteady velocity potential
h	modified unsteady velocity potential
h_l, h_t	h associated with leading and trailing edges, respectively
$H_{0,1,2,3}$	terms in inner expansion of h
k	aerodynamic reduced frequency
kw	acoustic reduced frequency
k_0	ω/c_0
L	scarfing angle

$\mathcal{L}_{0,1}$	operators in wave equation (2.4)
M_∞	upstream Mach number
N^\pm	upper and lower surfaces of blade
P	power level (equation (4.5))
p'	acoustic pressure
p_{mn}	duct pressure eigenmode
r, θ	plane polar coordinates
r_{mn}	radius of caustic cylinder in duct
\mathcal{S}	acoustic source strength
U_∞	upstream steady flow speed
\mathbf{v}'	vortical part of unsteady velocity
x, y, z	Cartesian coordinates
α	cascade stagger
β_∞	$\sqrt{1 - M_\infty^2}$
Δ	cascade spacing
δ	ordering parameter for blade thickness and camber
δp	phase distortion
ϵ	small parameter
Θ	polar angle (see figure 9)
θ_{mn}	ray angle for cylindrical duct mode
θ_s^m	cascade mode angle
θ_t	polar angle relative to trailing edge
ϕ	velocity potential of steady flow
ϕ_{mn}	ray angle for cylindrical duct mode
φ	angular (azimuthal) coordinate
χ	mode angle in cascade inter-blade passage
ψ	stream function of steady flow
ρ_0	steady density
Σ	observer distance in ray coordinates
σ	ray eikonal (equation (2.8))
σ'	inter-blade phase angle (equation (3.1))
Ω	source phase term (equation (2.4))
Ω_{rot}	engine shaft-rotation rate
ω	temporal frequency

The author is very grateful to Dr G. Keith for helpful comments on the manuscript and for supplying some of the figures.

References

- Abbott, I. H. & von Doenhoff, A. E. 1959 *Theory of wing sections*. Dover.
 Atassi, H. M. & Grzedzinski, J. 1989 Unsteady disturbances of streaming motions around bodies. *J. Fluid Mech.* **209**, 385–403.

Phil. Trans. R. Soc. Lond. A (2004)

- Atassi, H. M., Subramaniam, S. & Scott, J. R. 1990 Acoustic radiation from lifting airfoils in compressible subsonic flow. AIAA paper no 90-3911. Reston, VA: American Institute of Aeronautics and Astronautics.
- Chapman, C. J. 1994 Sound radiation from a cylindrical duct. 1. Ray structure of the duct modes and of the external field. *J. Fluid Mech.* **281**, 293–311.
- Chapman, C. J. 1996 Sound radiation from a cylindrical duct. 2. Source modelling, nil-shielding directions, and the open-to-ducted transfer function. *J. Fluid Mech.* **313**, 367–380.
- Cooper, A. J. & Peake, N. 2001 Propagation of unsteady disturbances in a slowly varying duct with mean swirling flow. *J. Fluid Mech.* **445**, 207–234.
- Durbin, P. A. 1983a High-frequency Green-function for aerodynamic noise in moving-media. 1. General theory. *J. Sound Vib.* **91**, 519–525.
- Durbin, P. A. 1983b High-frequency Green-function for aerodynamic noise in moving-media. 2. Noise from a spreading jet. *J. Sound Vib.* **91**, 527–538.
- Evers, I. & Peake, N. 2002 On sound generation by the interaction between turbulence and a cascade of airfoils with non-uniform mean flow. *J. Fluid Mech.* **463**, 25–52.
- Ffowcs Williams, J. E. & Hawkings, D. L. 1969 Sound generation by turbulence and surfaces in arbitrary motion. *Phil. Trans. R. Soc. Lond. A* **264**, 321–342.
- Goldstein, M. E. 1976 *Aeroacoustics*. New York: McGraw-Hill.
- Goldstein, M. E. 1978 Unsteady vortical and entropic distortions of potential flows round arbitrary obstacles. *J. Fluid Mech.* **89**, 433–468.
- Golubev, V. V. & Atassi, H. M. 1998 Acoustic-vorticity waves in swirling flows. *J. Sound Vib.* **209**, 203–222.
- Golubev, V. V. & Atassi, H. M. 2000 Unsteady swirling flows in annular cascades. 1. Evolution of incident disturbances. *AIAA J.* **38**, 1142–1149.
- Hinch, E. J. 1991 *Perturbation methods*. Cambridge University Press.
- Hocter, S. T. 2000 Sound radiated from a cylindrical duct with Keller's geometrical theory. *J. Sound Vib.* **231**, 1243–1256.
- Keith, G. M. 2000 A theoretical investigation into the acoustic radiation from an aeroengine intake. PhD thesis, University of Cambridge, UK.
- Keith, G. M. & Peake, N. 2002a High-wavenumber acoustic radiation from a thin-walled axisymmetric cylinder. *J. Sound Vib.* **255**, 129–146.
- Keith, G. M. & Peake, N. 2002b High-wavenumber acoustic radiation from a thin-walled scarfed cylinder. *J. Sound Vib.* **255**, 147–160.
- Keller, J. B. 1962 Geometrical theory of diffraction. *J. Opt. Soc. Am.* **52**, 116–130.
- Kerrebrock, J. L. 1977 Small disturbances in turbomachine annuli with swirl. *AIAA J.* **15**, 794–803.
- Kerschen, E. J. & Balsa, T. F. 1981 Transformation of the equation governing disturbances of a two-dimensional compressible flow. *AIAA J.* **19**, 1367–1370.
- Lee, S. W. 1978 Path integrals for solving some electromagnetic edge diffraction problems. *J. Math. Phys.* **19**, 1414–1422.
- Lighthill, M. J. 1952 On sound generated aerodynamically. I. General Theory. *Proc. R. Soc. Lond. A* **221**, 564–587.
- Lighthill, M. J. 1954 On sound generated aerodynamically. II. Turbulence as a source of sound. *Proc. R. Soc. Lond. A* **222**, 1–32.
- Lighthill, M. J. 1956 Drift. *J. Fluid Mech.* **1**, 31–53.
- Ludwig, D. 1966 Uniform asymptotic expansions at a caustic. *Commun. Pure Appl. Math.* **19**, 215–250.
- Myers, M. R. & Kerschen, E. J. 1995 Influence of incidence angle on sound generation by airfoils interacting with high-frequency gusts. *J. Fluid Mech.* **292**, 271–304.

- Myers, M. R. & Kerschen, E. J. 1997 Influence of camber on sound generation by airfoils interacting with high-frequency gusts. *J. Fluid Mech.* **353**, 221–259.
- Noble, B. 1988 *Methods based on the Wiener–Hopf technique*. New York: Chelsea.
- Peake, N. 1992 The interaction between a high-frequency gust and a blade row. *J. Fluid Mech.* **241**, 261–289.
- Peake, N. & Cooper, A. J. 2001 Acoustic propagation in ducts with slowly varying elliptic cross-section. *J. Sound Vib.* **243**, 381–401.
- Peake, N. & Kerschen, E. J. 1995 A uniform approximation for unsteady cascade flow. *Proc. R. Soc. Lond. A* **449**, 177–186.
- Peake, N. & Kerschen, E. J. 1997 Influence of mean loading on noise generated by the interaction of gusts with a flat-plate cascade: upstream radiation. *J. Fluid Mech.* **347**, 315–346.
- Peake, N. & Kerschen, E. J. 2004 Influence of mean loading on noise generated by the interaction of gusts with a cascade: unsteady lift and downstream radiation. *J. Fluid Mech.* (Submitted.)
- Rienstra, S. W. 1999 Sound transmission in slowly varying circular and annular lined ducts with flow. *J. Fluid Mech.* **380**, 279–296.
- Rienstra, S. W. 2003 Sound propagation in slowly varying lined ducts of arbitrary cross section. *J. Fluid Mech.* **495**, 157–173.
- Rienstra, S. W. & Eversman, W. 2001 A numerical comparison between multiple-scales and finite-element solution for sound propagation in lined flow ducts. *J. Fluid Mech.* **437**, 367–384.
- Scott, J. R. & Atassi, H. M. 1995 A finite-difference, frequency-domain numerical scheme for the solution of the gust response problem. *J. Computat. Phys.* **119**, 75–93.
- Tam, C. K. W. & Auriault, L. 1998 The wave modes in ducted swirling flows. *J. Fluid Mech.* **371**, 1–20.
- Tsai, C. 1992 Effect of airfoil thickness on high-frequency gust interaction noise. PhD thesis, University of Arizona, Tucson, AZ, USA.
- Weinstein, L. A. 1969 *The theory of diffraction and the factorization method*. Boulder, CO: Golem Press.
- Zhang, X., Chen, X. X., Morfey, C. L. & Tester, B. J. 2003 Computation of fan noise radiation through a realistic engine exhaust geometry with flow. AIAA paper no. 2003-3267. Reston, VA: American Institute of Aeronautics and Astronautics.